EPR SPECTRA OF IRON CENTERS IN SYNTHETIC QUARTZ: RADIATION AND HEAT EFFECTS

By

PATRICK EDWARD FISANICH

Bachelor of Science
Lamar University
Beaumont, Texas
1979

Master of Science
Lamar University
Beaumont, Texas
1980

Submitted to the Faculty of the Graduate College
of the Oklahoma State University
in partial fulfillment of the requirements
for the Degree of
MASTER OF SCIENCE
December, 1983

EPR SPECTRA OF IRON CENTERS IN SYNTHETIC QUARTZ:

RADIATION AND HEAT EFFECTS

Thesis Approved:

Larry E. Halliburton

Thesis Adviser

W. A. Sibley

Norman N. Durham

Dean of the Graduate College

ACKNOWLEDGMENTS

The author thanks Dr. L. E. Halliburton for his help and understanding. Without his kindly assistance this thesis would not have been completed. Appreciation is also expressed to Dr. W. A. Sibley and Dr. E. E. Kohnke for serving on the Committee. The assistance of K. L. Sweeny in my learning how to use various pieces of equipment and for proper scientific approach to the experiments is most appreciated.

TABLE OF CONTENTS

Chapter		Page
I.	INTRODUCTION	1
	Quartz	1
	Basic Structure	1
	Physical Properties	6
	Defects in Quartz	6
	Point Defects	6
	Iron in Quartz	9
	Amethyst and Citrine	9
	Origin of Color	10
	Effect of Heat on Coloration	10
	Effect of Radiation on Coloration	11
	Previous EPR Studies in Iron-Doped Quartz	11
	Present Study	18
II.	EXPERIMENTAL PROCEDURE	21
	Samples	21
	EPR Spectrometer	21
	Sample Arm	23
	Detector	23
	Output	23
	Bias Arm	24
	Microwave Source	24
	Microwave Frequency Counter	24
	Modulation	24
	Variable-Temperature Irradiations	24
III.	EXPERIMENTAL RESULTS	27
	As-Received	27
	Irradiation Study	29
	Anneal Study	32
IV.	DISCUSSION	40
	The Problem	40
	Proposed Model	41
	Suggestions for Further Research	41
A SELECTED BIBLIOGRAPHY		43

LIST OF FIGURES

Figure		Page
1.	The Trigonal Crystal Structure of α-Quartz.	3
2.	Orientation of the SiO_4 Tetrahedra in Quartz.	4
3.	View Along the C Axis of Right-Handed Quartz.	5
4.	Charge-Compensated Aluminum Defect Centers.	8
5.	Schematic Representation of S_1 Center	14
6.	Model for the Formation of the Amethyst Color Center by Radiation	16
7.	Schematic Representation of I Center.	17
8.	Model for the Formation of the Amethyst Color Center by Heat.	19
9.	Block Diagram of EPR Spectrometer	22
10.	Block Diagram of Variable Temperature Irradiation Experiment.	25
11.	EPR Spectrum for the S_1 Center.	28
12.	EPR Spectrum After 250 K Irradiation.	30
13.	EPR Spectrum for the Aluminum-Hole Center After 250 K Irradiation	31
14.	EPR Spectrum for the R Center	33
15.	EPR Spectrum After 520 K Anneal	34
16.	EPR Spectrum After 680 K Anneal	35
17.	Composite of EPR Spectra.	36
18.	Irradiation Study of the S_1 and R Centers	38
19.	Anneal Study of the S_1 and R Centers.	39
20.	Schematic Representation of Iron and Aluminum Centers. Radiation-Induced Mobility of Alkali Interstitials.	42

CHAPTER I

INTRODUCTION

The crystalline state of the silicates has been particularly studied because they are frequently found in nature as crystals and because of their industrial importance. The particular polymorph of silica called low,or alpha quartz,is the most common form of these substances and is one of the major constituents of the Earth's crust. The name quartz was first used in the Middle Ages in Saxony for massive veins, and not until the late eighteenth century did the name quartz become identified with all the colored varieties of this mineral.

Quartz

Basic Structure

Quartz is composed of oxygen and silicon ions in a nearly perfect tetrahedral structure. Each silicon is surrounded by four oxygens and each oxygen links two silicons. Strong covalent bonds connect the silicon and oxygen ions. The negative charge (approximately one minus) on each of the oxygen ions is compensated by the positive charge (appproximately two positive) on each of the silicon ions, so the total crystal remains charge neutral.

During growth of the quartz crystals in nature (1), isolated single SiO_4 tetrahedra are first formed above the melting temperature. The number of these tetrahedra increase as the temperature decreases and

competition for the cations in the melt leads to an insufficient number of available oxygen ions to saturate all the silicon ions. Therefore, several tetrahedras will combine together by sharing an oxygen ion as a bridging formation, with one common vertex. This leads to chains of SiO_4 tetrahedras and establishment of a crystal structure.

Much of the quartz material used today is grown in a laboratory by the hydrothermal technique (2). Pressures of approximately 20,000 psi and temperatures near 350°C are needed. Natural quartz crystals are placed in the bottom of the autoclave for nutrient and one or more seeds are suspended in the upper portion of the autoclave. A temperature gradient of approximately 10-20°C is maintained between the lower and upper regions. Quartz crystals typically take two weeks to two months to grow.

Alpha-quartz has a trigonal crystal structure. The symmetry elements are a single three-fold axis (or optic axis) and three two-fold axes perpendicular to the optic or c axis. These latter three axes, labeled a_1, a_2, and a_3 are 120° degrees apart and define the basal plane. Figure 1 illustrates these symmetry elements. A Cartesian coordinate system is defined in terms of these crystallographic axes as follows: x is in the $+a_1$ direction, z is along the optic axis, and y is such as to complete a right hand system. The four digit numbers in Figure 1 identify the crystal faces.

As previously stated, the SiO_4 tetrahedra are not perfect. The four oxygens surrounding a silicon are divided into two types: long Si-O bonds of 1.612 Å and short Si-O bonds of 1.607 Å (3). The basic SiO_4 tetrahedron is shown in Figure 2. The unit cell of quartz contains three silicon sites on different levels along the c axis. Figure 3

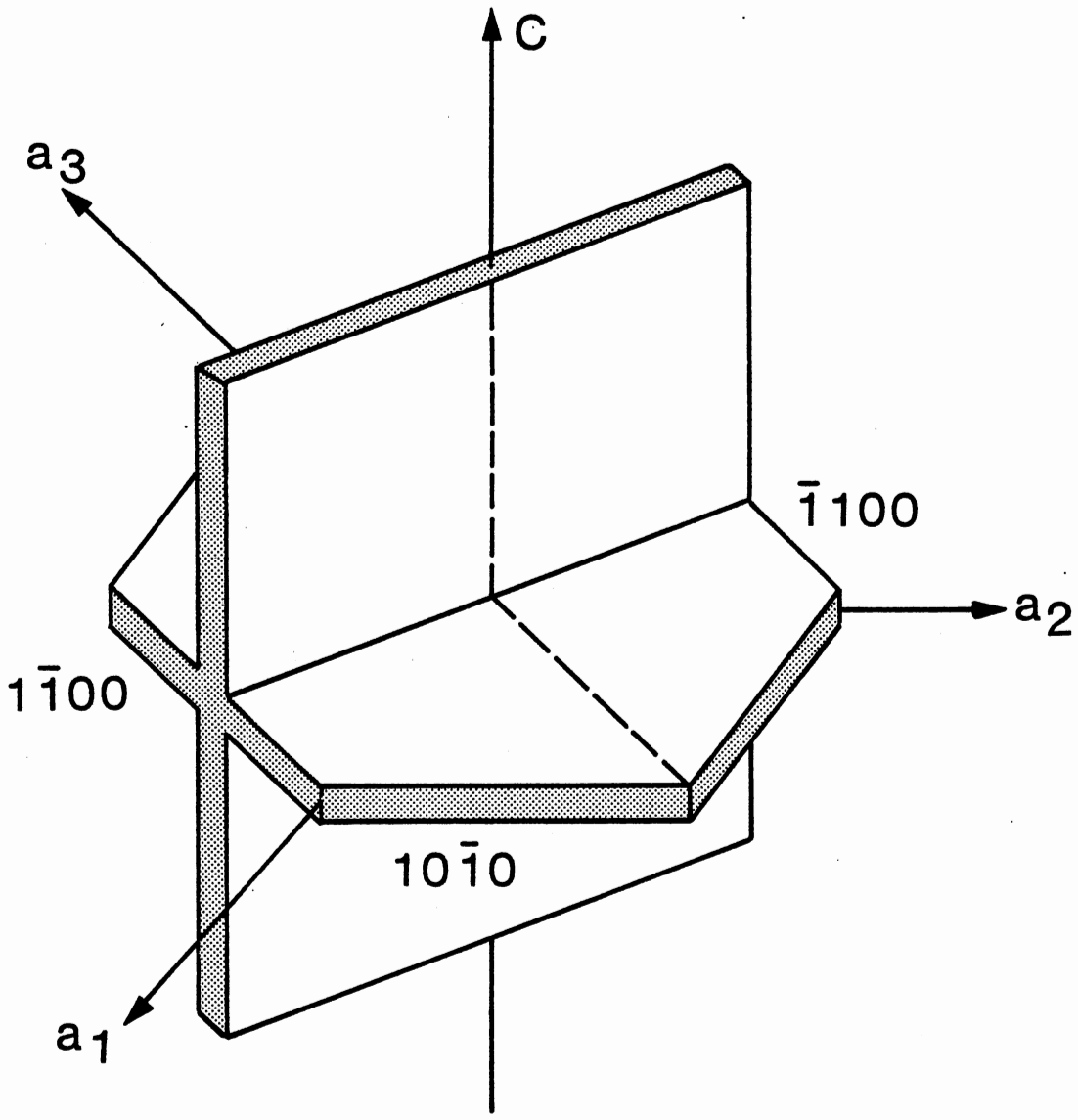

Figure 1. The Trigonal Crystal Structure of α-Quartz

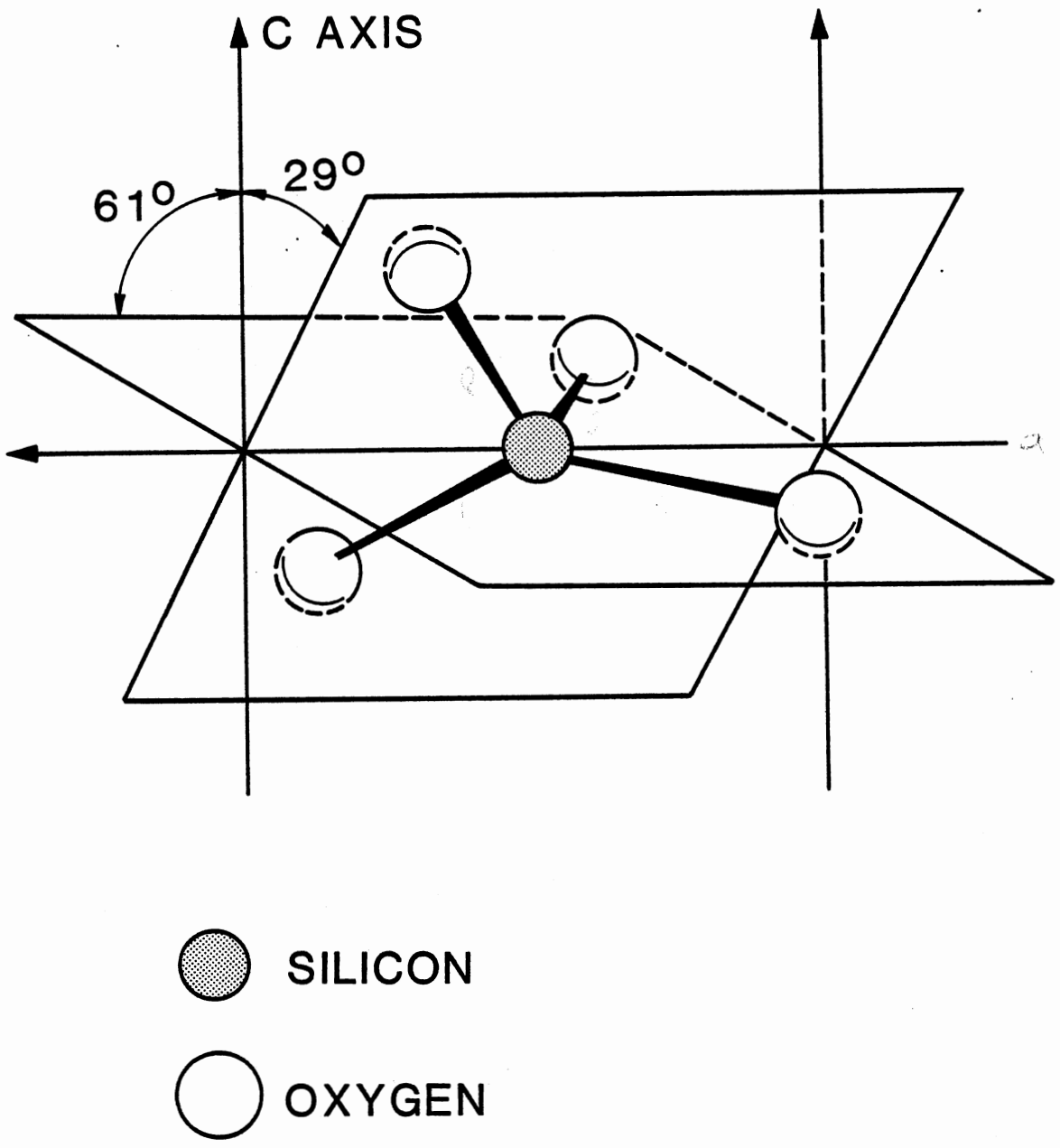

Figure 2. Orientation of the SiO_4 Tetrahedra in Quartz

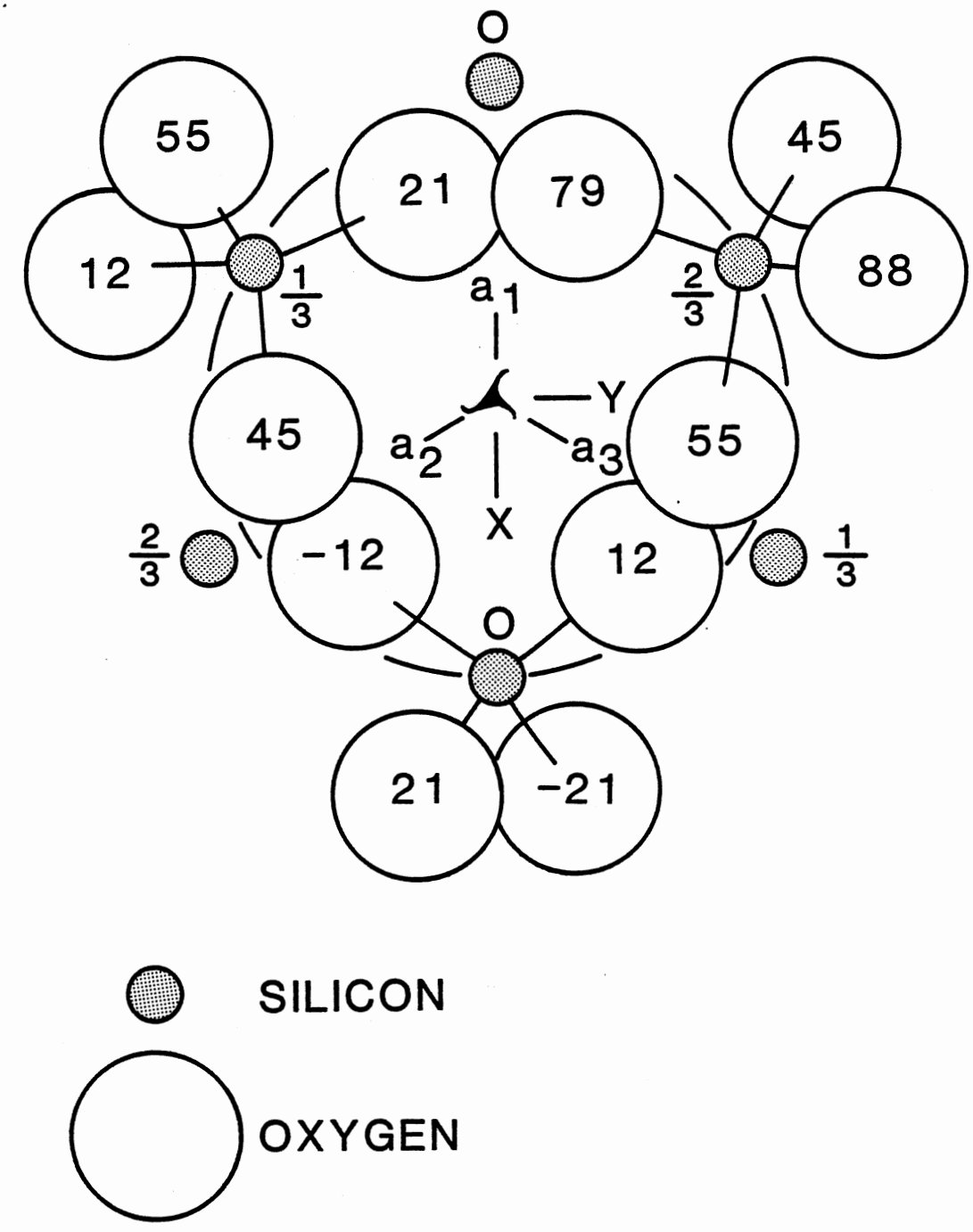

Figure 3. View Along the C Axis of Right-Handed Quartz

shows the quartz lattice looking down the c axis. The numbers beside the silicon atoms are the heights above the basal plane in fractions of c_o, the lattice parameter. The numbers inside the oxygen atoms give the height of the oxygen atoms above the basal plane in hundredths of c_o.

Physical Properties

The most important physical property of quartz is its piezoelectric behavior (5, 6). Piezoelectricity results when a crystal is noncentrosymmetric and is manifested by an induced electric polarization when a crystal is subjected to an external mechanical stress. This property of quartz has led to many applications in the general area of precision frequency control. Another useful property of quartz is its wide band gap. This makes quartz a widely used optical material, especially in the ultraviolet region of the spectrum.

Defects in Quartz

Point Defects

A variety of defects in solids may be produced either during the growth or introduced later by the application of various forces, i.e., radiation, mechanical, thermal, etc. Examples of extended defects are dislocations and inclusions while point defects are the result of the addition of impurities or the absence or misplacement of ions in an otherwise perfect region of the crystal. Most of the early work on point defects was done in simpler structures such as the alkali halides (7) and alkaline-earth oxides (8). In particular, electron paramagnetic resonance (EPR) has proven to be one of the most important techniques for obtaining an exact knowledge of the electronic structure and the

local environment of a point defect, provided of course that it is paramagnetic (9).

In insulators such as quartz, point defects are known as color centers because they usually have two or more electronic states lying within the band gap between which transitions are possible. The complex crystal structure of quartz, the presence of the aluminum and interstitial alkali impurities, and the presence of hydrogen and growth-induced oxygen vacancies all combine in making quartz susceptible to formation of a variety of point defects. High energy radiation, i.e., x-rays, gamma rays, electrons, etc., produce electron-hole pairs and allow these charges to be trapped at many different sites in the crystal. A significant number of these defects have an unpaired electron and can be studied with EPR. Insight to the defect behavior can be gained by monitoring the EPR spectra during irradiations at different temperatures, during optical bleaching, and during thermal anneals.

Aluminum impurities are found in all quartz (4). These are Al^{3+} ions that substitute for the Si^{4+} ions. This leaves a net negative charge at this site in the crystal which is compensated by an interstitial monovalent impurity ion such as Li^{+}, Na^{+}, or H^{+}. Much of the recent work on defects in quartz has focused on the behavior of the aluminum and its interstitial charge compensators.

Figure 4 shows the various aluminum-associated centers previously investigated in quartz (4). These are the $Al\text{-}OH^{-}$ center which is easily detected by infrared absorption (10). Next is the $Al\text{-}M^{+}$ center, where M^{+} represents Li^{+} or Na^{+}, and is detected by acoustic loss in the case of Na^{+} (11). Finally, we have the $Al\text{-}h^{+}$ center which is detected by EPR. If the crystals are irradiated above 200 K, the interstitial Li^{+}

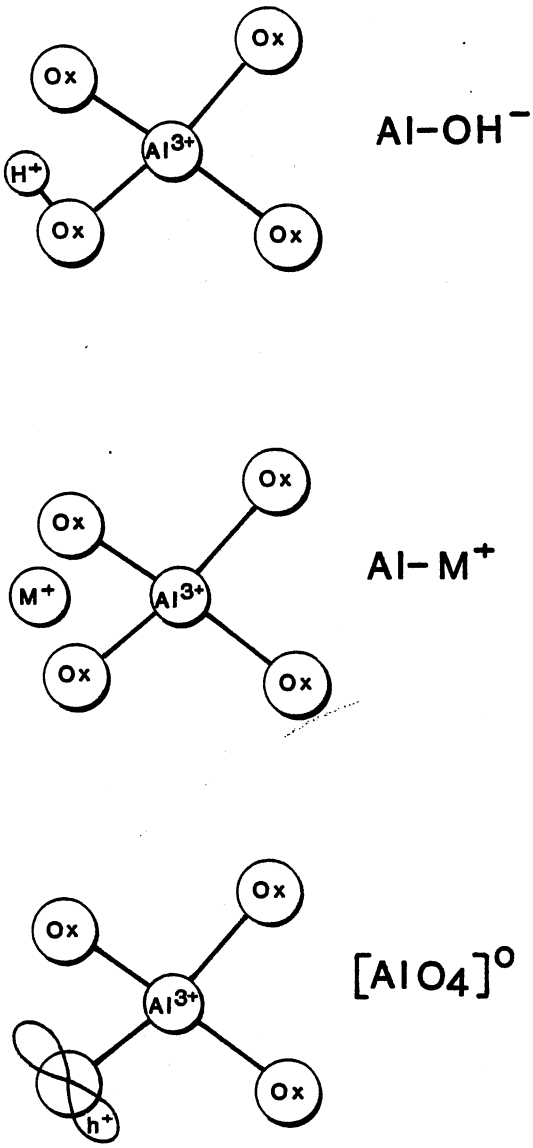

Figure 4. Charge-Compensated Aluminum Defect Centers

or Na^+ ions will move away from the aluminum ion and leave a hole trapped on one of the oxygen ions in the aluminum tetrahedron (12). Hydrogen atoms are formed by radiation at low temperatures, but thermally decay near 125 K (13).

Another family of point defects in quartz is the oxygen-vacancy-associated centers, commonly known as E centers. The E_1' center has been most widely studied and is believed to be a single oxygen vacancy with an unpaired electron trapped in an sp^3 hybrid orbital extending into the vacancy from an adjacent silicon ion (14). Two additional centers, the E_2' and E_4', are similar oxygen-vacancy centers except that they have a proton associated with them (15, 16).

Iron in Quartz

Amethyst and Citrine

Natural quartz that is high in iron content is known by the mineralogical names of amethyst and citrine. These crystals are semiprecious gemstones. The color of amethyst ranges from shades of violet to purplish violet, the color of citrine varies from yellow to brownish yellow. It is known that heat treatments turn amethyst to citrine.

The name amethyst is derived from Greek and means "not drunken." It was believed that the wearer was protected from the intoxicating effect of wine. Amethyst is mentioned in the Bible as one of the stones used by the Israelites to adorn the linen bag worn by the High Priest when ministering to Jehovah. The identification of amethyst as a variety of quartz was done in 1708 by J. J. Scheuchzer (17).

The name citrine comes from the French citrin, meaning lemon colored. Natural citrine is rare and is sometimes confused with topaz. Most citrine in the gem trade is made by the heat treatment of amethyst

which gives a reddish tint compared to natural citrine and is sometimes called "burnt amethyst."

Origin of Color

There has been much speculation about the cause of color in amethyst, but there is now a large body of circumstantial evidence that iron is responsible. The color is not usually distributed uniformly in the natural crystals but is observed to be in very thin layers parallel to the external faces, usually the r face and sometimes the r and z faces. The optical properties were first described by Brewster (18) in 1823. Frondell (19) in 1892 and Holden (20) in 1925 did much of the initial optical characterization work. Cohen (21) has shown that iron is always present in amethyst and has summarized the various possibilities of iron incorporation. The amount of iron in amethyst is considerably greater than the amount of aluminum.

Brazil twinning is common in natural amethyst crystals and liquid-filled inclusions are often found. The iron itself may be present as an adsorbed phase, colloidally dispersed, substitutional for silicon, or in interstitial positions. The variation of physical properties and cell dimensions for amethyst are unknown. It is believed that amethyst forms at relatively lower temperature and pressure than does smoky or rose quartz.

Effect of Heat on Coloration

It has been known for hundreds of years that amethyst can be decolored, i.e., bleached, or changed to a citrine color by heat treatments. The rate of decoloration increases with increasing temperature

above 300°C. The results of the heat treatments on amethyst vary considerably with annealing time and crystal but generally follow this pattern:

1. No change in color up to 300°C.
2. Color bleached out at 400°C.
3. Previously violet regions become yellow-brown at 500°C.
4. Yellow-brown regions turn milkly translucent at 600°C.
5. Above the 573°C phase transition, it becomes either clear, milky, or opalescent.

Some amethyst has no colorless stage, while Madagascar amethyst turns colorless but never citrine. Amethyst from Minas Gerais, Brazil turns green when heated in air and colorless when heated in hydrogen to 550°C. Some amethyst will phosphoresce on heating. Colorless or smoky quartz usually does not develop the milky stage at high temperatures.

Effect of Radiation on Coloration

Berhelof in 1906 discovered that amethyst or citrine that was bleached by heat could be restored by irradiation with x-rays emitted from a natural radioactive source (22). The full nature and behavior of the color centers in iron-doped quartz has not yet been determined. The present investigation is an attempt to use radiation to perturb the iron centers and, thus, reveal their identities.

Previous EPR Studies in Iron-Doped Quartz

Hutton (23) studied amethyst and citrine at both X and K bands. He plotted energy levels versus magnetic field up to 12 kG for the magnetic

field parallel to the c axis and then indicated the positions of the resonant transitions. The EPR spectrum with the magnetic field parallel to the c axis gave signals with linewidths of four gauss at room temperature and two gauss at 77 K. Hutton found identical EPR spectra for amethyst, citrine, and heat-treated amethyst that had turned yellow. The three equivalent sites had magnetic axes related to, but not equal to, the crystallographic axes. In a right hand system, the results were $x = a_1$, y perpendicular to a_1 and making a 30^o angle with the c axis, and z perpendicular to a_1 and making a 57^o angle with the c axis. He concluded that the iron ion was Fe^{3+} substitutional for Si^{4+} and charge compensated by a positive interstitial impurity. He suggested that iron, Brazil twinning, and high-energy radiation were all responsible for the violet amethyst color.

Hutton and Troup (24) studied amethyst and citrine from 9 to 16 kG. In natural citrine, a broad isotropic EPR line about 100 G wide near 12.2 kG was observed whose intensity is proportional to the depth of the yellow-brown color. Both this EPR line and the color reached a maximum intensity for annealing temperatures in the 600-700^{o}C range and annealed out near 1000^{o}C. When natural amethyst is annealed at about 540^{o}C, the violet areas turn yellow-brown and the broad isotropic EPR line appears. Hutton and Troup attributed this to Fe^{3+} in amorphous surroundings. Three highly populated sites, besides those reported by Hutton (23), were found with magnetic axes rotated 60^o from the c axis. With heat treatment above the alpha-beta phase transition temperature, the line strengths of the two sets of sites become nearly equal, presumably because of diffusion of Fe^{3+} or alkali interstitials. The ratio of line intensities of weak and strong sites was 400 before annealing, then 100

after 500°C for 15 hours, and finally 1.3 after annealing at 700°C for 15 hours. Two other EPR centers, not related to crystallographic axes in a simple way, were also reported by Hutton and Troup. These were not found in all amethyst and no explanation of these centers was given.

Barry and Moore (25) studied amethyst at X band. They determined the angular variation of a prominent Fe^{3+} center for rotation about an a_1 axis. At 0°, i.e., the magnetic field parallel to the c axis, a five-line spectrum was found with components approximately at 833, 1751, 2140, 3603, and 4963 gauss. The angular variation showed that the spectrum is strongly anisotropic with an axial distortion along the twofold axis but with a still stronger orthorhombic distortion possibly caused by a charge-compensating ion on the twofold axis. The angular data showed that three equivalent Si^{4+} sites are unequally occupied by Fe^{3+} with intensities in the order 10 : 1.2 : 0.8. The twofold axis corresponding to the center having the highest concentration is the same as that for the color and the optical biaxiality of the crystal. The color was bleached by heat treatments in air at 400°C and restored with x- or gamma-ray irradiation. The EPR intensity increased slightly with heat treatment up to 400°C. This showed that the magnetic centers are not the color center, but act as a precursor and can be converted to the color center with ionizing radiation. They concluded that all the iron was Fe^{3+} substitutional for Si^{4+}. Figure 5 shows their model.

Barry, McNamara, and Moore (26) made X band measurements on three Brazilian amethysts and orange-brown synthetic quartz. This was a more detailed study than Barry and Moore (25) with considerably more optical work being included for the amethysts. Their synthetic quartz was grown by Sawyer. Again, an EPR five-line spectrum with a strong central line

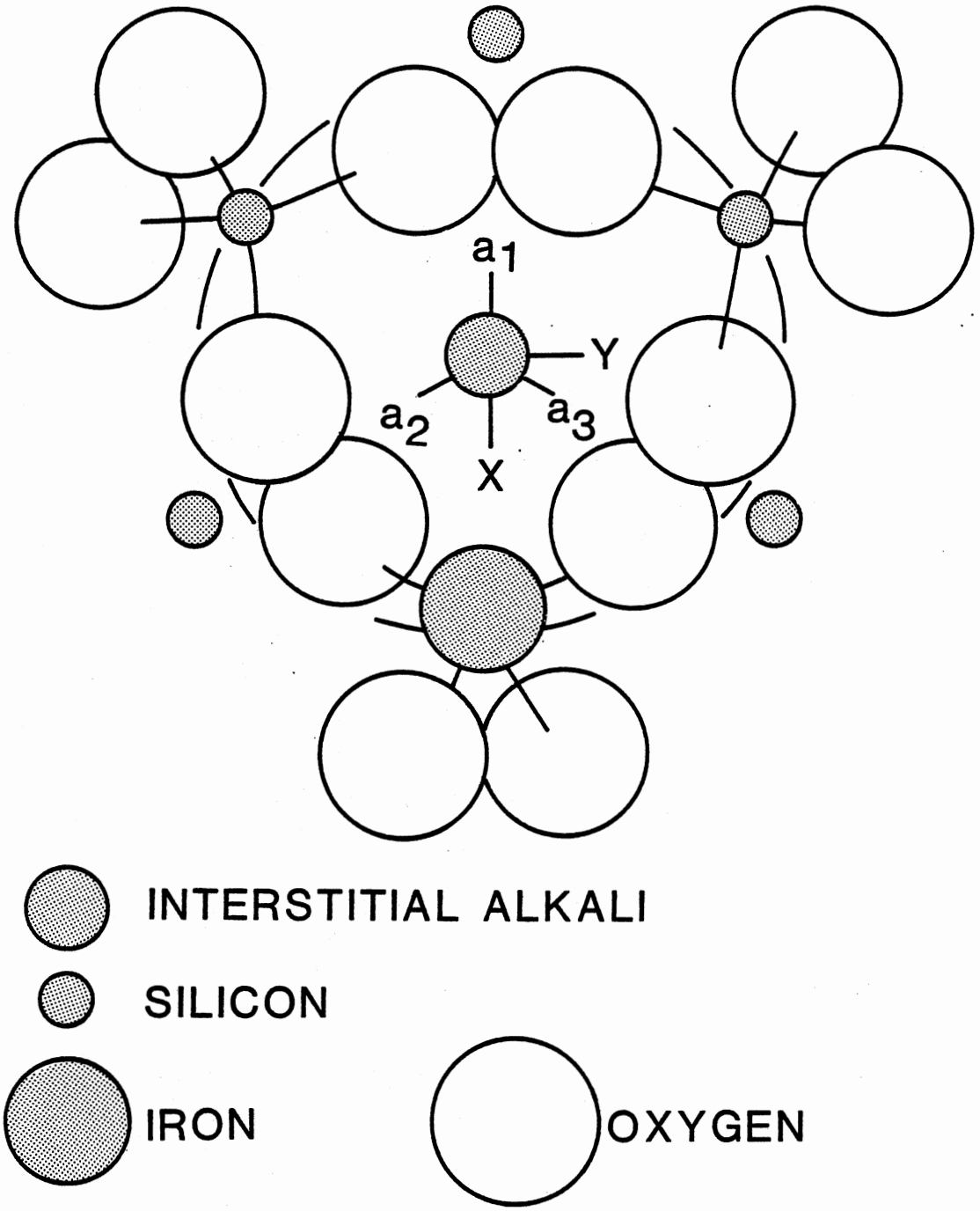

Figure 5. Schematic Representation of S_1 Center

at g = 2 was observed and had peaks identical with the most prominent peaks in natural amethyst. However, the linewidths were greater in the synthetic samples. X-ray irradiation of the orange-brown quartz showed amethyst coloration in very thin surface regions under the r faces. Three EPR peaks in the synthetic quartz coincided with peaks in the 500°C heat-treated amethyst which had turned orange-brown and lost the aluminum-hole spectrum. They offered the same defect model as before with an explanation of the paramagnetic centers being a precursor to the color centers, both having similar symmetry. Figure 6 shows their mechanism for the formation of the color center in amethyst by radiation. In this model, the sodium ion never diffuses away, a hole is trapped on one or more of the oxygen ions, and an electron is added to the lattice.

Matarrese, Wells, and Peterson (27) studied synthetic brown quartz and natural amethyst at both X and K bands. All EPR measurements were done at room temperature with most signals being in the 5-10 kG range for K band. Both synthetic brown and green quartz gave the same five-line spectrum centered at g = 2 with lines located at 4500, 6100, 7800, 9600, and 11300 gauss plus many extra lines usually found in the natural amethyst spectrum. The five-line spectrum had intensities of 5 : 8 : 9 : 8 : 5, a different crystal field axes system, and a smaller zero field splitting than the amethyst crystal. They also found an unequal distribution of Fe^{3+} ions in amethyst. This five-line EPR spectrum was labeled S_1 and is assigned to a substitutional Fe^{3+} ion charge compensated by an interstitial alkali ion. A different EPR spectrum was also found in the synthetic brown quartz and has been labeled the I center. This latter center was suggested to be an interstitial Fe^{3+} ion charge compensated by a substitutional alkali ion. Figure 7 shows the model for this I center.

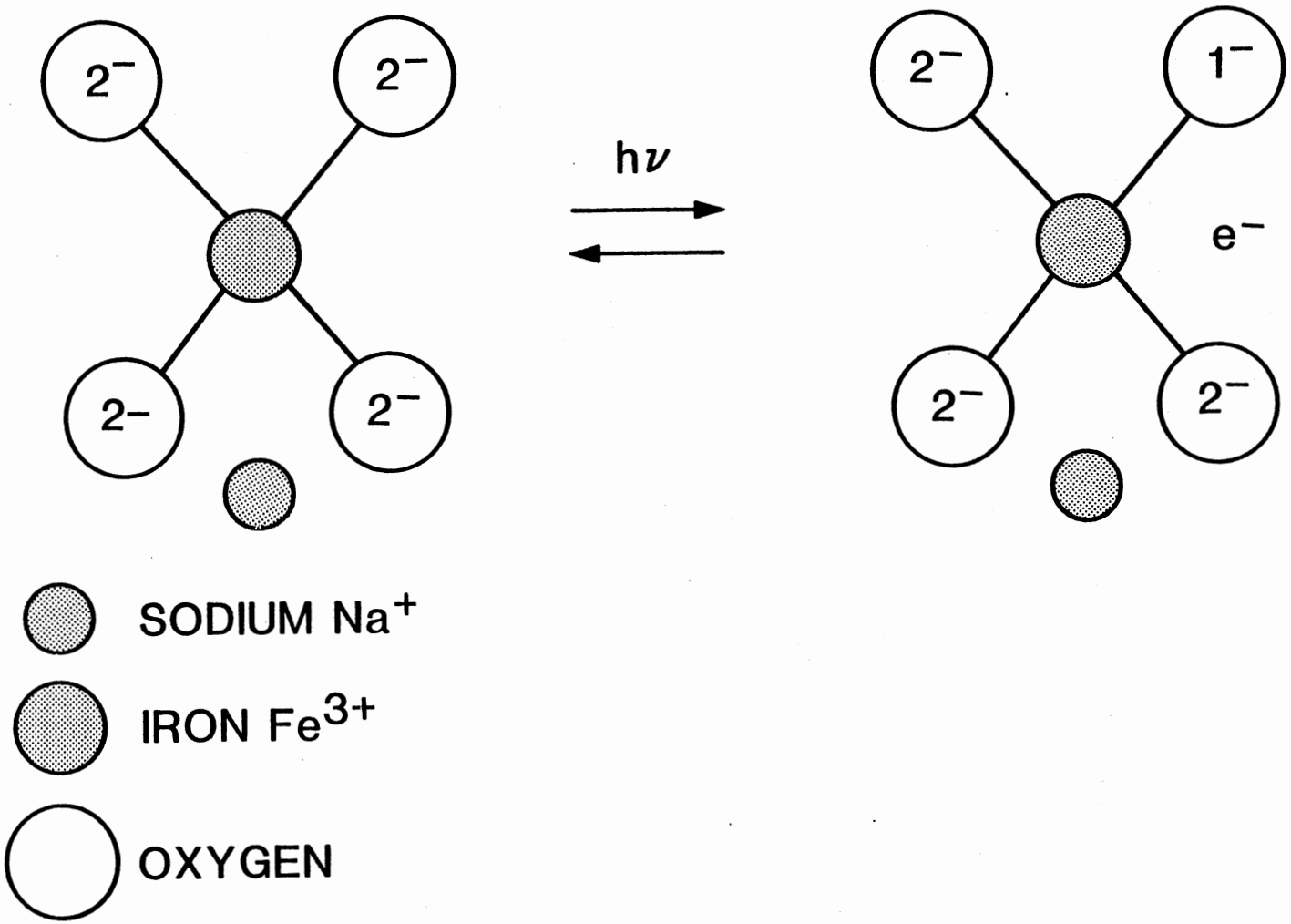

Figure 6. Model for the Formation of the Amethyst Color Center by Radiation

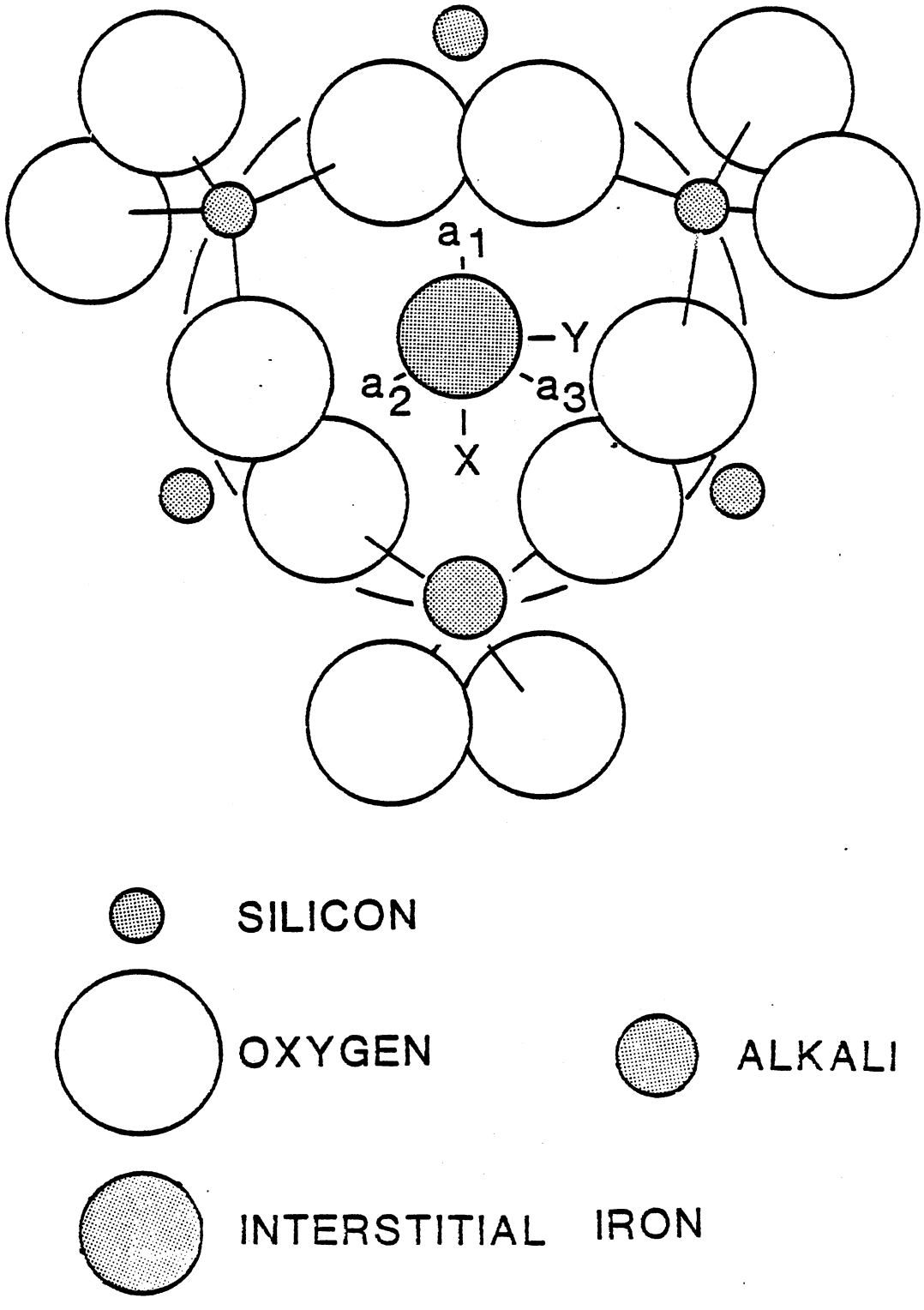

Figure 7. Schematic Representation of I Center

Lehman and Moore (28) made X band measurements on synthetic brown and green quartz grown by Sawyer. With the c axis normal to the magnetic field the EPR spectrum was a very regular five-line spectrum for both colors of quartz. The EPR lines were at 300, 1750, 3500, 5100, 6750 gauss. They believe this to be the spectrum of an I center. They concluded that the brown synthetic quartz has interstitial Fe^{3+} and that amethyst has substitutional Fe^{2+}. Figure 8 shows their proposed mechanism for the change in color of brown to violet quartz.

Cox (29) measured the optical absorption of natural amethyst. He concluded from his and also Lehmann and Moore's (28) data that the iron was incorporated as a substitutional Fe^{4+} ($3d^4$) ion at a silicon site. This $(FeO_4)^{4-}$ molecule results from the effect of room temperature gamma ray radiation on Fe^{3+} ions.

Present Study

The primary purpose of the present study is to determine the effects of high energy electrons (1.7 MeV) on synthetic iron-doped quartz. Previous investigators have suggested Fe^{3+} is substitional, in analogy to aluminum. Also, it has been shown that the interstitial charge compensating alkalis migrate away from the aluminum during irradiation above 200 K. Our goal was to observe the difference in the iron EPR spectra as a result of irradiation and determine if iron behaved like aluminum, at least with regard to charge compensator mobility. To find the temperature at which this proposed onset of charge-compensating ion migration occurs, a variable-temperature irradiation experiment was done on the iron-doped samples. The radiation-induced centers will usually be stable up to some critical temperature and then decay to their original

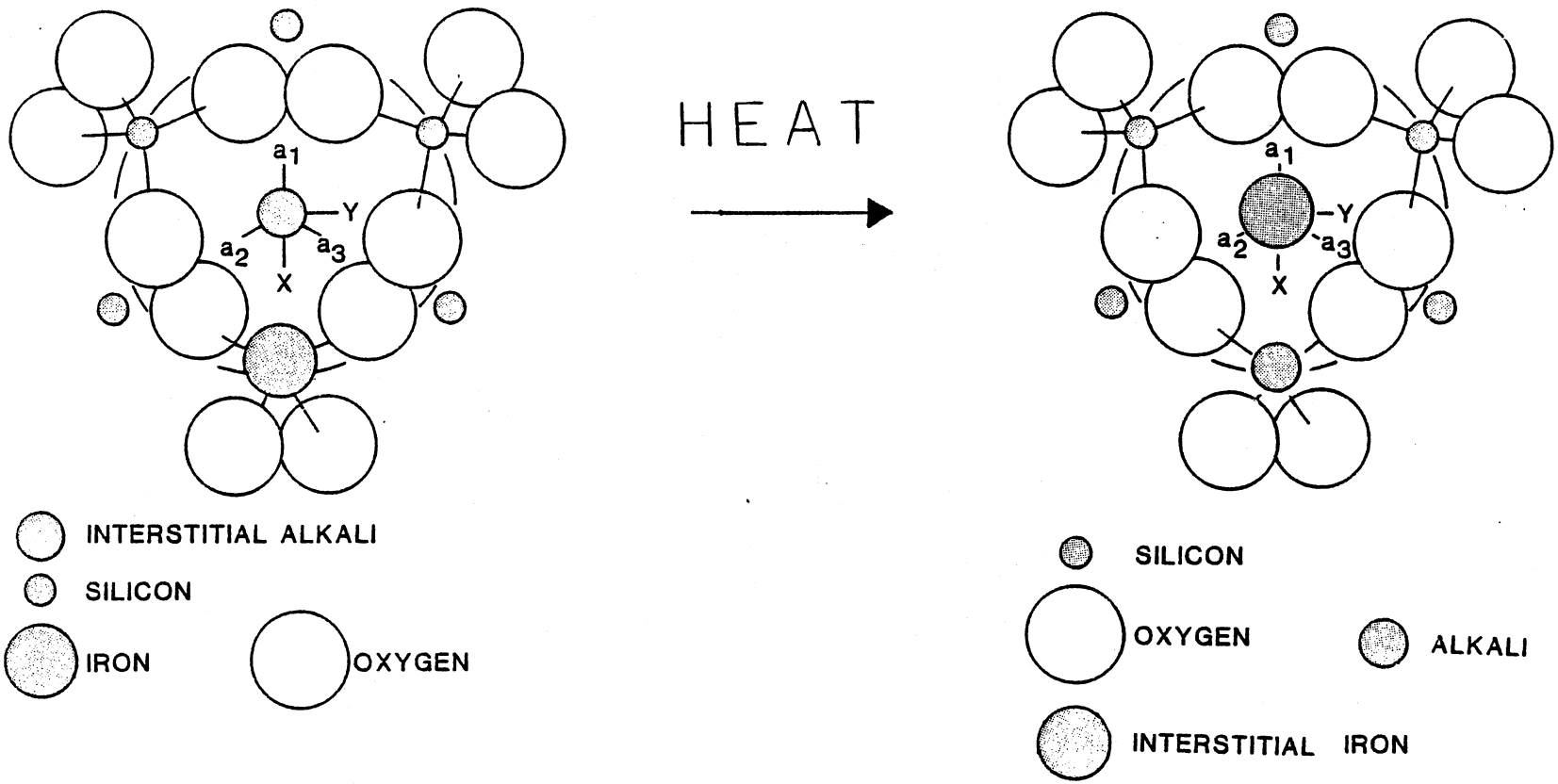

Figure 8. Model for the Formation of the Amethyst Color Center by Heat

configuration. Therefore, a thermal annealing experiment was done after the variable-temperature irradiation experiment. All EPR spectra were taken with the magnetic field parallel to the c axis and at 77 K.

CHAPTER II

EXPERIMENTAL PROCEDURE

Samples

The synthetic yellow quartz used in this study was kindly given to us by Sawyer Research Products, Eastlake, Ohio, and consisted of a large single crystal approximately 3 x 3 x 3 cm^3. A thin area perpendicular to the axis was of a slightly lighter color of yellow. Samples suitable for the EPR studies were cut from this crystal with dimensions of approximately 10 x 3 x 2 mm^3 in the X, Y, and Z directions, respectively.

In order to incorporate iron into isolated sites in the quartz during growth, a fast growth rate is used by Sawyer. This rate is typically a factor of five greater than for high grade material to be used in quartz oscillators. A detrimental effect of the fast growth rate is the significant amount of strain found in the iron-doped quartz.

EPR Spectrometer

All EPR measurements were taken on a Varian 4502A X-band spectrometer at 77 K. Figure 9 is a block diagram of the spectrometer showing the component parts that generate and control the microwave photon radiation. Also shown are the detector and output parts that detect and display absorption of the applied radiation by the sample. The following is a brief listing of the numbered boxes in the figure and a de-

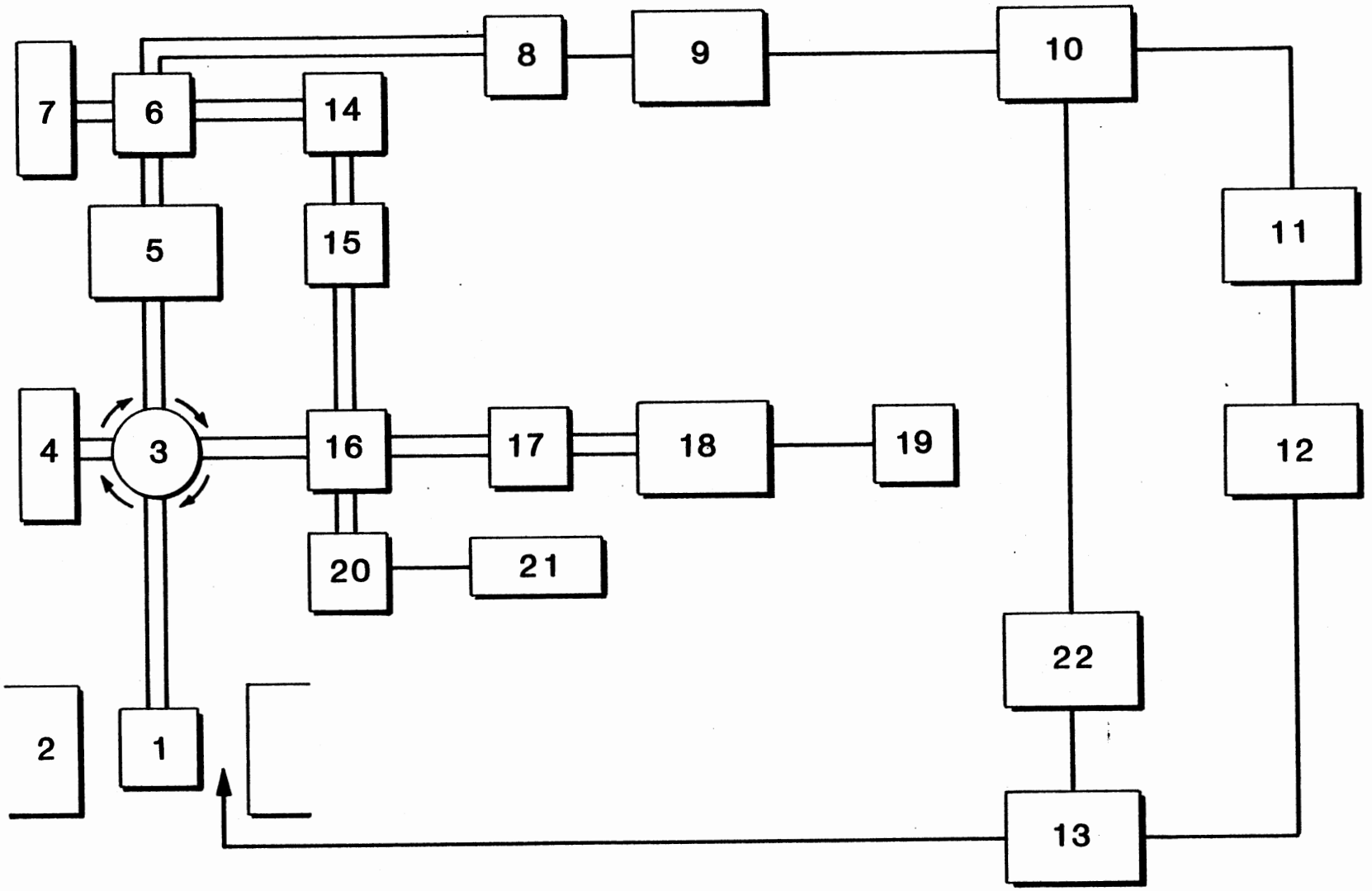

Figure 9. Block Diagram of EPR Spectrometer

scription of each component.

Sample Arm

1. Cavity: The sample cavity is a rectangular parallelipiped operating in the TE_{102} mode. Coupling of the microwave energy into the cavity is achieved by adjusting an iris screw.
2. Electromagnet: A Varian 9-inch V-7200 electromagnet produces a static magnetic field that is amplitude modulated at 100 kHz.
3. Circulator: A circulator is used to direct microwave power to the cavity and to direct the reflected signal from the cavity to the detector.
4. Load: A microwave absorber.
5. Microwave Amplifier: A GaAs FET solid state amplifier (Narda N6244S-37).
6. Magic Tee
7. Load

Detector

8. Tunable Diode Detector: A sensitive low-noise Schottky barrier diode (MA-40075).
9. 100 kHz Amplifier
10. Phase-Sensitive Detector

Output

11. Oscilloscope: Vertical input.
12. X-Y Recorder; Houston Instruments Model 2000.
13. Audio Sweep Generator

Bias Arm

14. Microwave Phase Shifter
15. Microwave Attenuator
16. Magic Tee
17. Microwave Isolator

Microwave Source

18. Klystron: Microwave power source (Model VA-153C from Varian), frequency adjusted to match the resonant frequency of the sample cavity.
19. Klystron Power Supply

Microwave Frequency Counter

20. Waveguide-to-Coax Adapter
21. Microwave Frequency Counter: Hewlett Packard Model 5340A.

Modulation

22. 100 kHz Modulation Oscillator

Variable-Temperature Irradiations

Figure 10 shows the block diagram of the variable-temperature irradiation set-up. The high-energy radiation was produced by a Van de Graaff accelerator operating at 1.7 MeV and 10 microamps. The sample was irradiated for four minutes at a fixed temperature and then a second four minute irradiation was done at 77 K to insure complete populating of the electron states. EPR data were taken at 77 K after the 77 K irradiation. Temperature control was improved by minimizing the distance

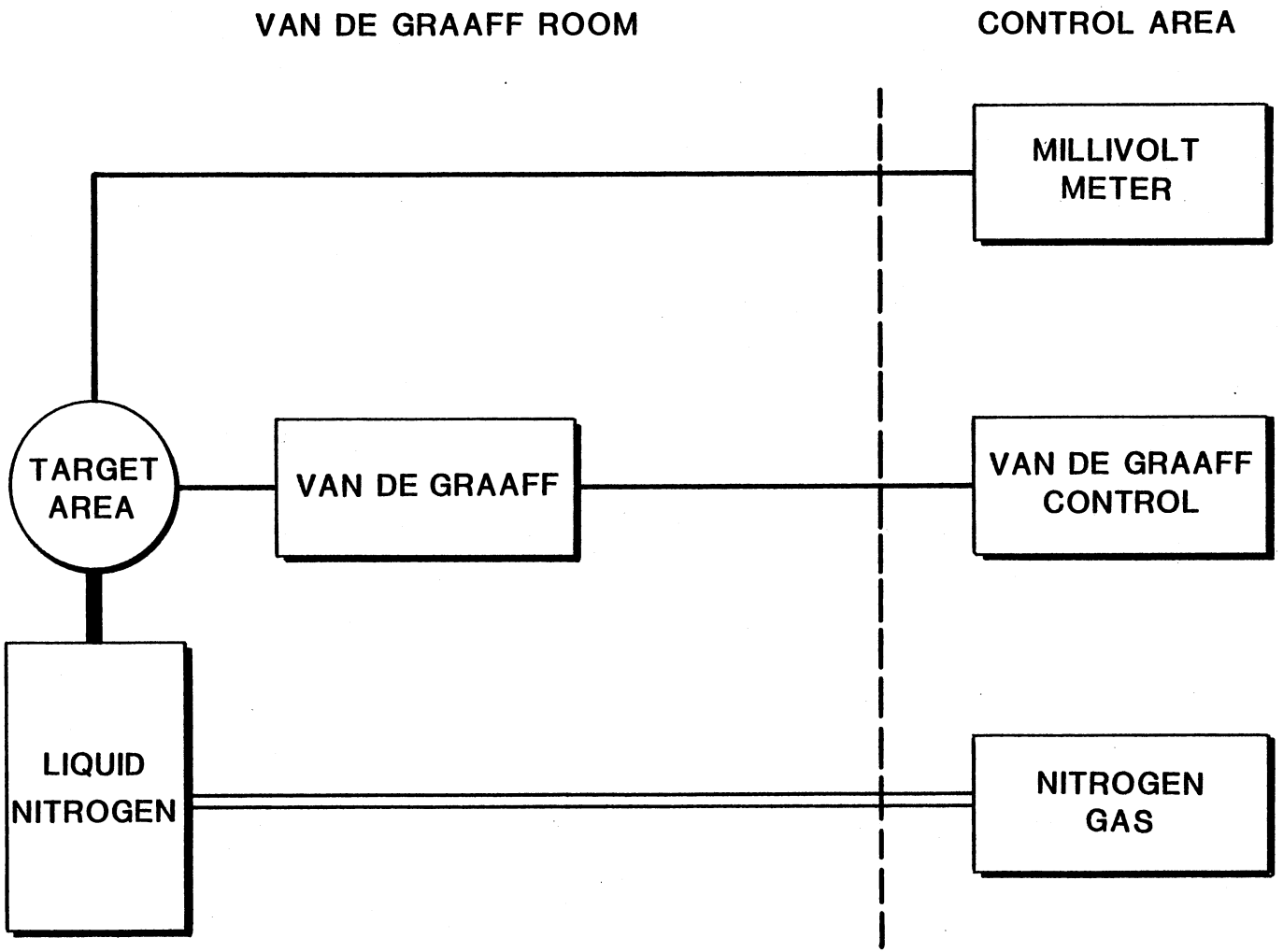

Figure 10. Block Diagram of Variable Temperature Irradiation Experiment

between the sample (in its glass tube) and the top of the liquid nitrogen. This distance was less than 7 cm. The irradiation temperature was carefully monitored from outside the Van de Graaff enclosure by observing a digital millivolt meter connected to a thermocouple below the sample. The nitrogen gas flow was adjusted to insure constant irradiation temperatures. The 77 K irradiations were done by placing the sample in a styrofoam cup filled with liquid nitrogen.

CHAPTER III

EXPERIMENTAL RESULTS

As-Received

The EPR spectrum from an as-received iron-doped quartz sample is shown in Figure 11. The microwave frequency is 9.13 GHz, the magnetic field is along the c axis, and the measurement temperature is 77 K. There are four prominent EPR lines in the 0 to 5 kG region, as shown. A large peak is at 1752 gauss, two smaller peaks having similar intensities are at 833 and 2140 gauss, and a still smaller peak is at 3603 gauss. Several additional less intense lines are found above 5 kG, but are not shown in this figure. Weak lines from a different center are observed in the 1470 to 1605 gauss region. An important feature of all of these EPR lines is their extreme sensitivity to magnetic field alignment. A significant reduction in intensity or even a splitting into a number of components occurs with only a 0.1^{o} or less misalignment relative to the c axis.

The prominent lines shown in Figure 11 comprise the EPR spectrum previously assigned to the S_1 center (26). In support of this association, a partial angular dependence study was done on the spectrum in Figure 11 and it was found to agree with the earlier work (26). This S_1 spectrum has been assigned to substitutional Fe^{3+} with an adjacent interstitial charge compensator. In order to find additional information to either prove or disprove the proposed model for this S_1 center,

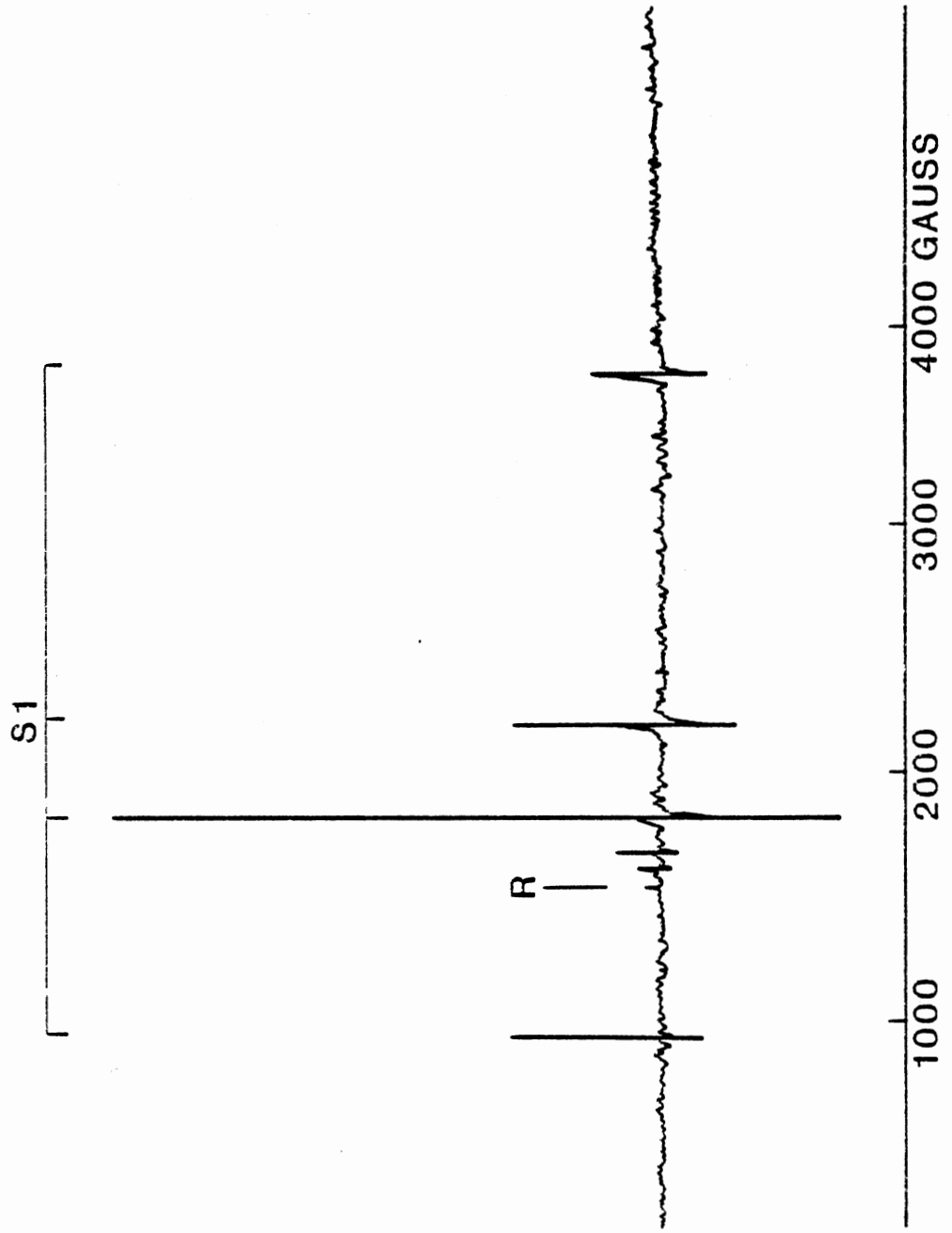

Figure 11. EPR Spectrum for the S_1 Center

we began a series of irradiations at temperatures between 77 K and room temperature and a series of thermal anneals from room temperature to near 550°C. It was hoped that we would find results that could be correlated with previous irradiation studies of aluminum-hole centers, i.e., radiation-induced mobility of alkali interstitials.

Irradiation Study

Irradiation at 77 K of an as-received sample has very little effect on the S_1 center. Other centers, such as the hydrogen atom (13) and aluminum-holes (12), are formed by the 77 K irradiation. However, if the irradiation temperature is increased, significant changes begin to occur. The intensity of the S_1 center decreases as a function of increasing irradiation temperature in the range 77 K to 170 K. No S_1 centers survive irradiations at temperatures above 170 K.

The number of aluminum-holes produced by irradiation increases by approximately a factor of two in the same temperature region where the S_1 center is decreasing. This is in contrast to undoped quartz where aluminum-holes increase more than an order of magnitude when the irradiation temperature exceeds 200 K (12). Figure 12 shows the effect of irradiating at 250 K. The S_1 center is gone and a prominent aluminum-hole spectrum is present. The aluminum-hole spectrum is enlarged in Figure 13.

As the S_1 centers are being destroyed by the increasing irradiation temperatures, a second group of lines increase in intensity. These lines are located in the 1470 to 1605 gauss region and were described in Figure 11. As the irradiation temperature increases to 250 K, these particular lines increase by more than a factor of five. We have found

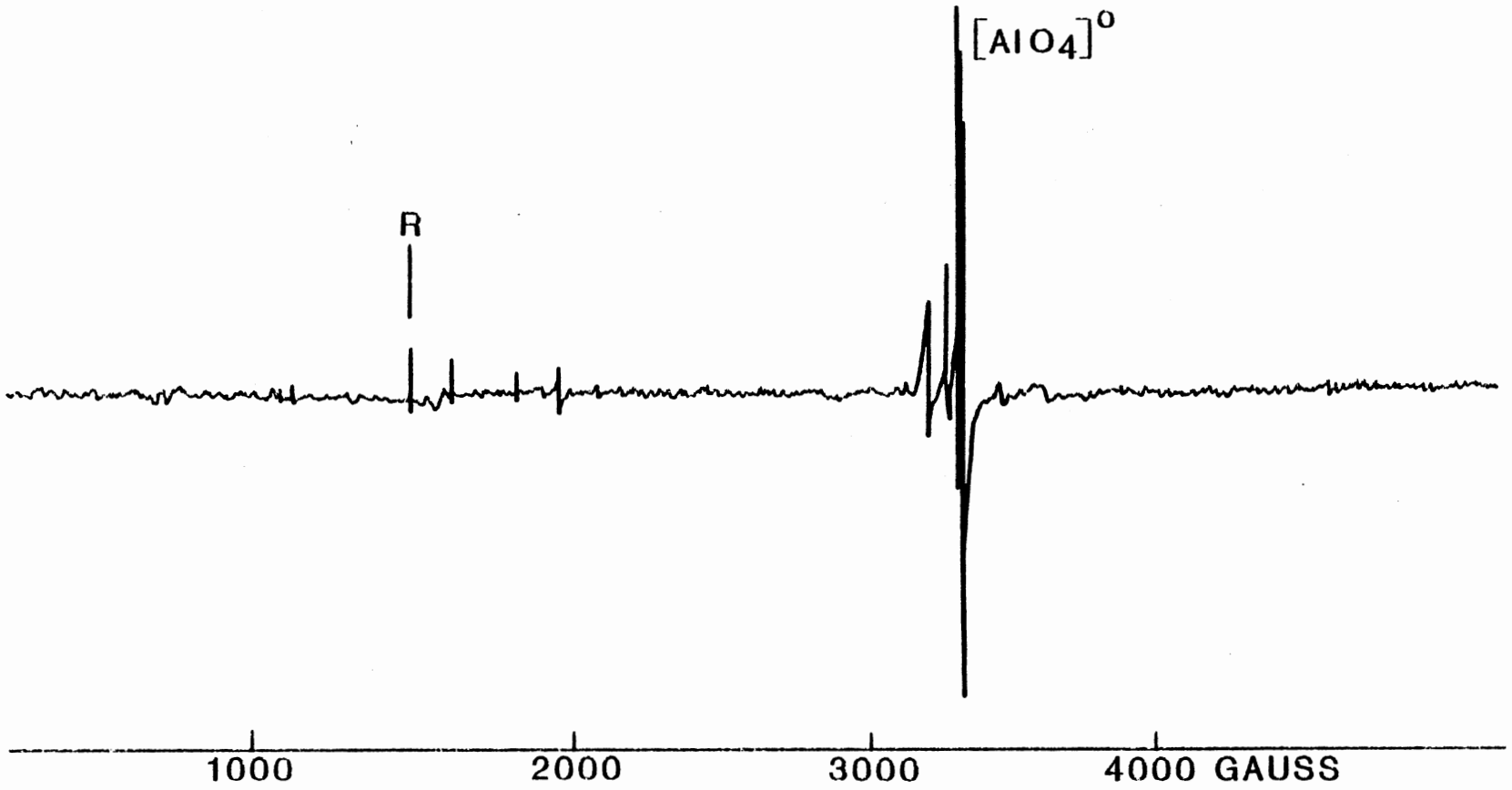

Figure 12. EPR Spectrum After 250 K Irradiation

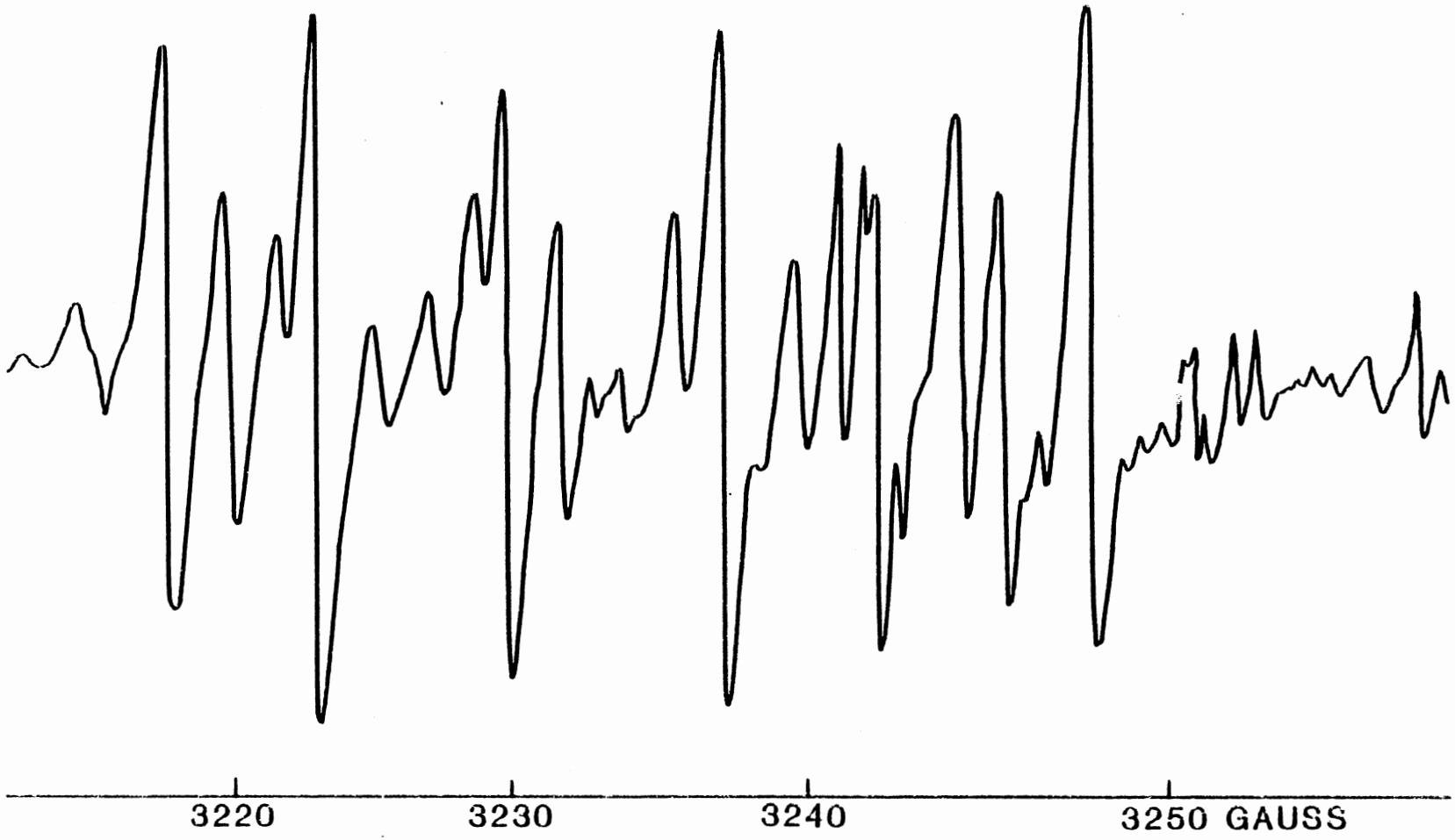

Figure 13. EPR Spectrum for the Aluminum-Hole Center After 250 K Irradiation

no references in the literature to this latter group of EPR lines.

Figure 14 is a 10 gauss sweep of the most intense peak in Figure 12 which we labeled R. This EPR spectrum is particularly sensitive to c axis alignment. There is some suggestion of structure found in these lines.

Anneal Study

After completing the variable-irradiation-temperature study between 77 K and room temperature, we began to anneal the irradiated sample above room temperature. The procedure was to heat to a desired temperature, hold the sample there for 15 minutes, and then cool back to room temperature. Following each anneal, the EPR spectrum of the sample was taken at 77 K.

Figure 15 shows the EPR spectrum after a 520 K anneal. The R center has increased greatly with heat treatments. The aluminum-hole center has decreased, and the intense lines to the lower field side of the aluminum-hole center have almost disappeared. Figure 16 shows the EPR spectrum after 680 K anneal. The R center is decreasing and the S_1 center is returning. Annealing to around 750 K brings back the S_1 center completely and destroys the R center as in Figure 11. The EPR spectrum of iron-doped synthetic quartz is "recyclable", i.e., the new EPR spectrum created by radiation can be annealed out, thus returning the sample to its original form. This follows the pattern of the aluminum center previously stated. Figure 17 is a composite of the 5 kilogauss EPR spectra taken during the irradiation and anneal experiments. Figure 17 is labeled as such: (a) S_1 center, (b) R center, (c) R center after 520 K anneal, (d) R_1 and S_1 center. What is most interesting is that

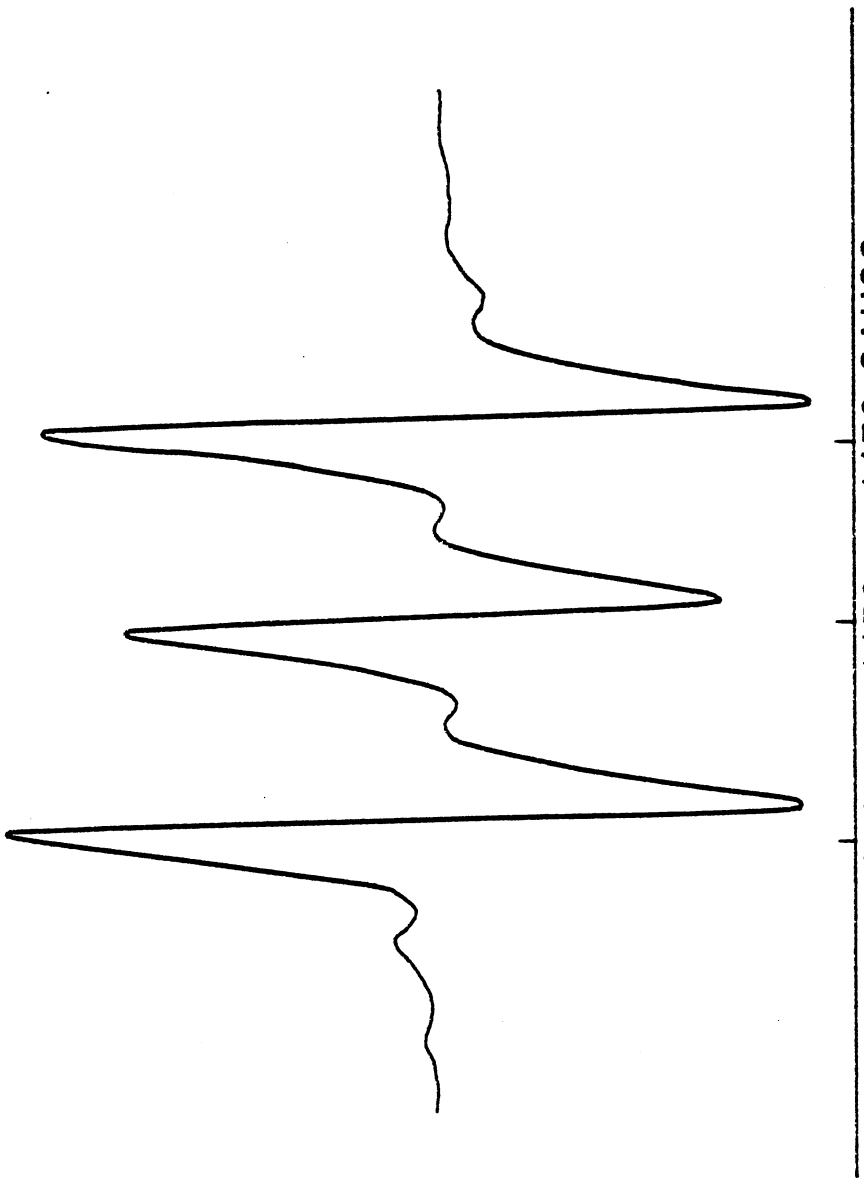

Figure 14. EPR Spectrum for the R Center

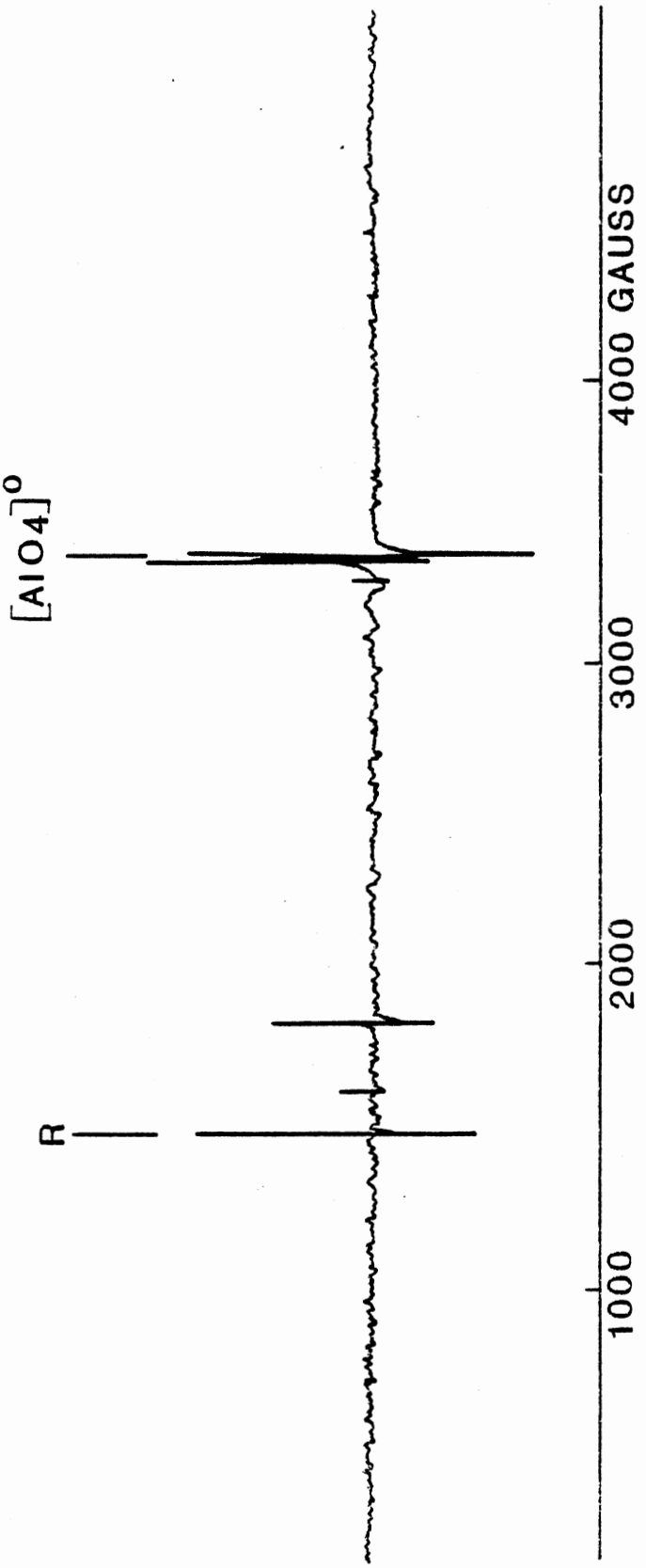

Figure 15. EPR Spectrum After 520 K Anneal

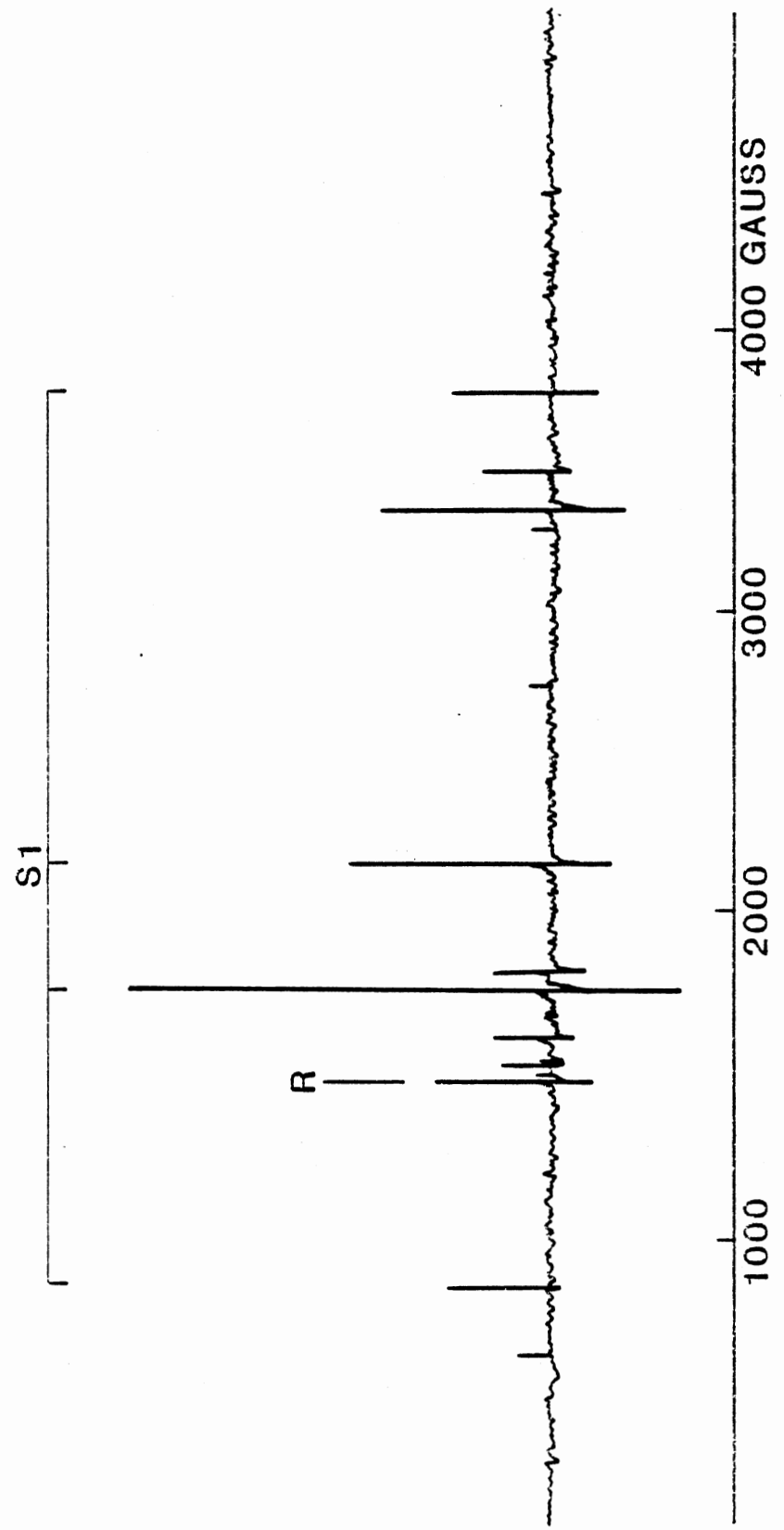

Figure 16. EPR Spectrum After 680 K Anneal

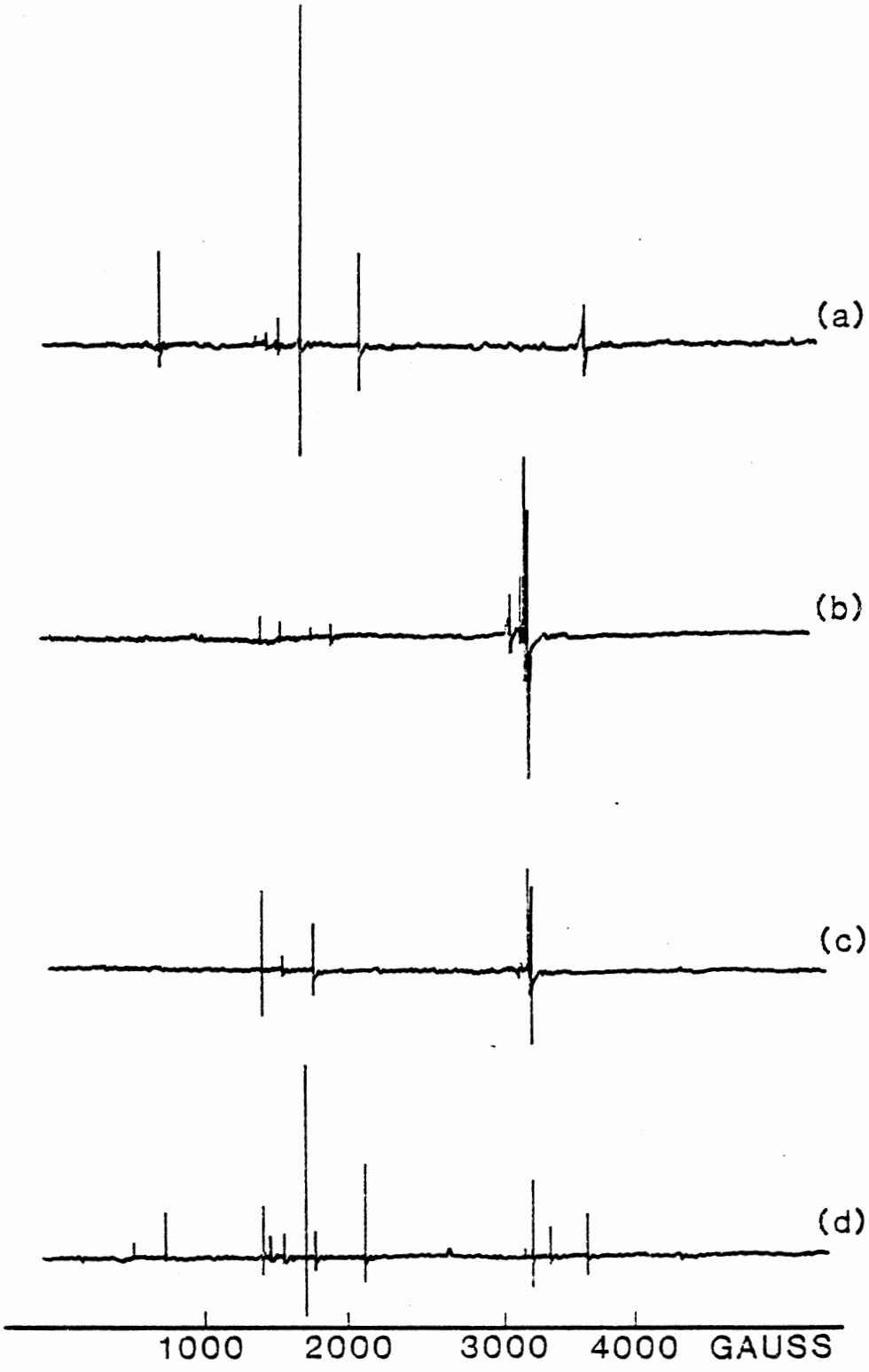

Figure 17. Composite of EPR Spectra

during the reappearance of the S_1 center as in (d) the S_1 center grows to two or three times its original intensity, as in (a), before returning to its original intensity.

Figure 18 shows plots of the intensity of the S_1, R, and aluminum center with increasing radiation temperature. Figure 19 shows the simultaneously decline of the R center and the growth of the S_1 center. Both graphs are normalized.

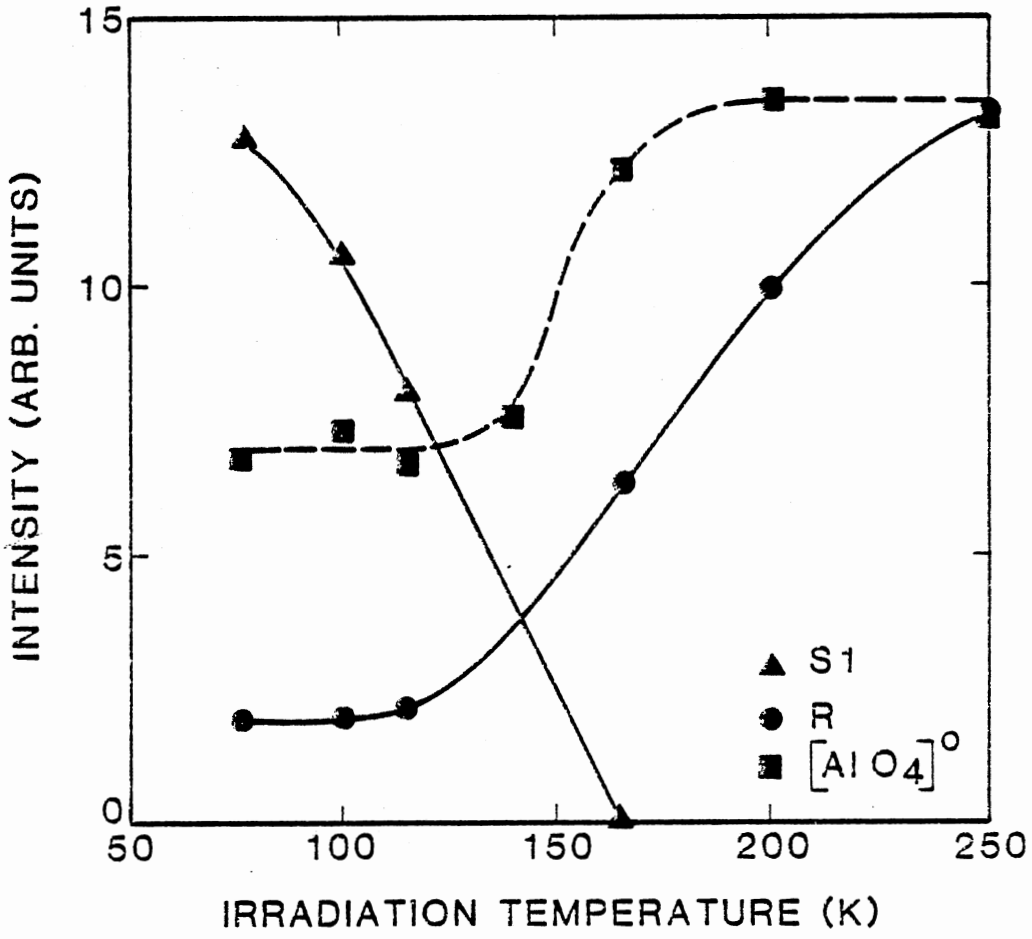

Figure 18. Irradiation Study of the S_1 and R Centers

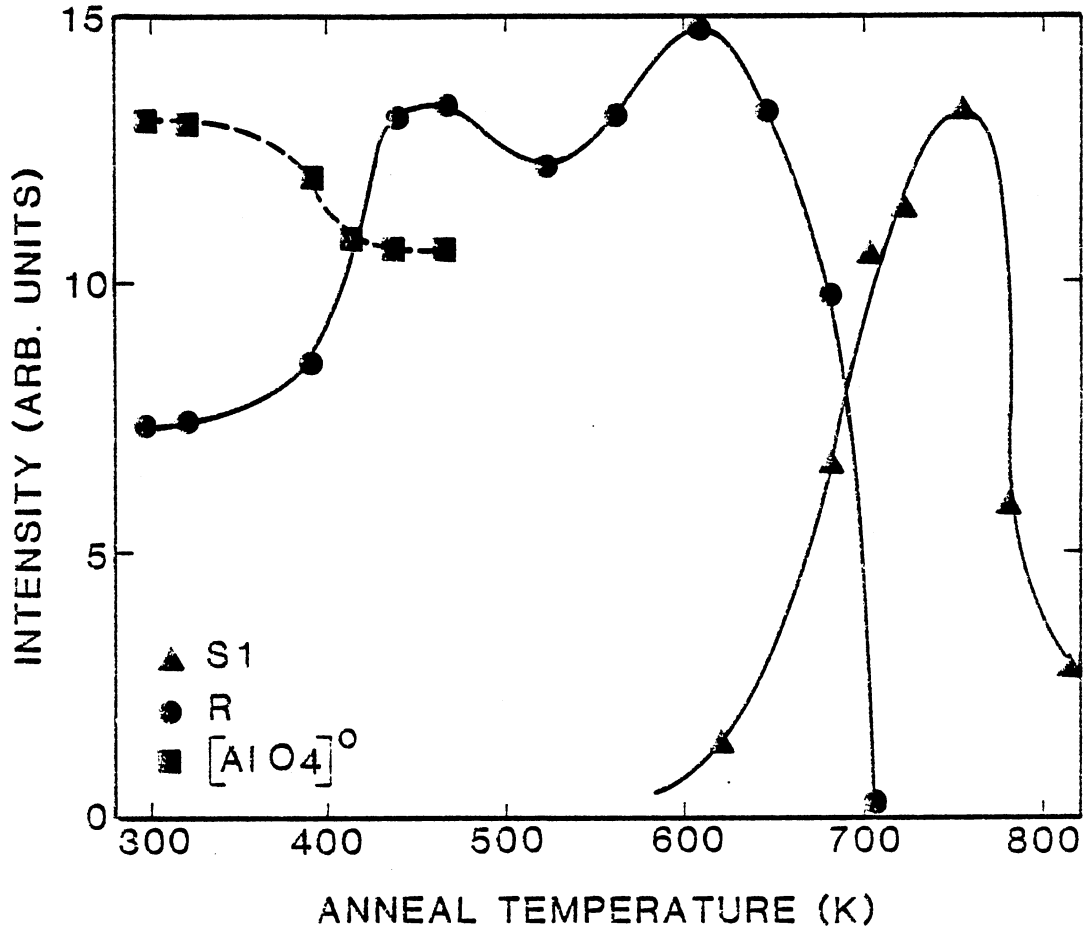

Figure 19. Anneal Study of the S_1 and R Centers

CHAPTER IV

DISCUSSION

The Problem

The question of which charge-species, Fe^{2+}, Fe^{3+}, or Fe^{4+}, the iron ion is in needs to be answered. The incorporation of the iron ion into the quartz lattice whether interstitial or substitional needs to be investigated. The role of any charge-compensating ion near the iron ion also should be examined.

The non-correlation of the S_1 and R centers during the irradiation experiment (Figure 18) would suggest that the two centers are not directly related. The R center growth at 125 K comes after the S_1 center decline at 100 K. It would seem that some large portion of the S_1 centers, maybe all of them, are being converted over to some nonparamagnetic state, in the zero to five kilogauss range. The possibility exists that we are not measuring all the paramagnetic states.

The correlation between the decline of the R center and the growth of the S_1 center at 675 K during the anneal experiments is most striking. This is strong evidence for the interconversion of R centers to S_1 centers. As mentioned earlier, during this repopulation of R and S_1 centers, the S_1 center signal increases by a factor of two to three times its original intensity before returning to its original value. The nature of these additional S_1 centers is most puzzling.

Proposed Model

The model which explains some of the properties of the iron defects is as follows. We believe that the iron ion $Fe^{3+}(3d^5)$ is incorporated into the SiO_2 structure as a substitute for silicon. The iron ion would be charge-compensated by a charge compensator ion which we assume to be an alkali, but could be hydrogen.

Figure 20 shows the behavior of the S_1 and substitional aluminum-associated center. Below 100 K irradiation has no effect on either the impurity defects iron or aluminum center. At irradiation temperatures at 100 K the electron-hole pairs are broken, with the hole migrating to the iron center. The hole is trapped by the Fe^{3+} ion creating a $Fe^{4+}(3d^4)$ ion and the electron is trapped on the alkali ion. Because Fe^{4+} is very difficult to detect with the EPR technique this results in no observable EPR spectrum. This would look like Figure 12. At irradiation temperatures above 150 K the aluminum centers behave in the same manner as the iron centers. This temperature is just slightly less than the usual temperature of 200 K in synthetic quartz. Annealing at 450 K reverses the process for the aluminum centers, which is less than the usual 600 K. The sodium ion moves back to charge compensate the aluminum center. At 700 K the charge compensating sodium ion moves back to the iron ion as in Figure 16. By 750 K the original S_1 iron spectrum has returned.

Suggestions for Further Research

An angular dependence study of the R center should be performed in order to obtain the $\vec{g}$ and $\vec{D}$ matrices. This data would tell us exactly the crystal parameters and allow a precise model to be proposed. Sweeping the crystal with hydrogen or sodium would also be quite useful. An ENDOR study would establish exactly what charge-compensating ion was present

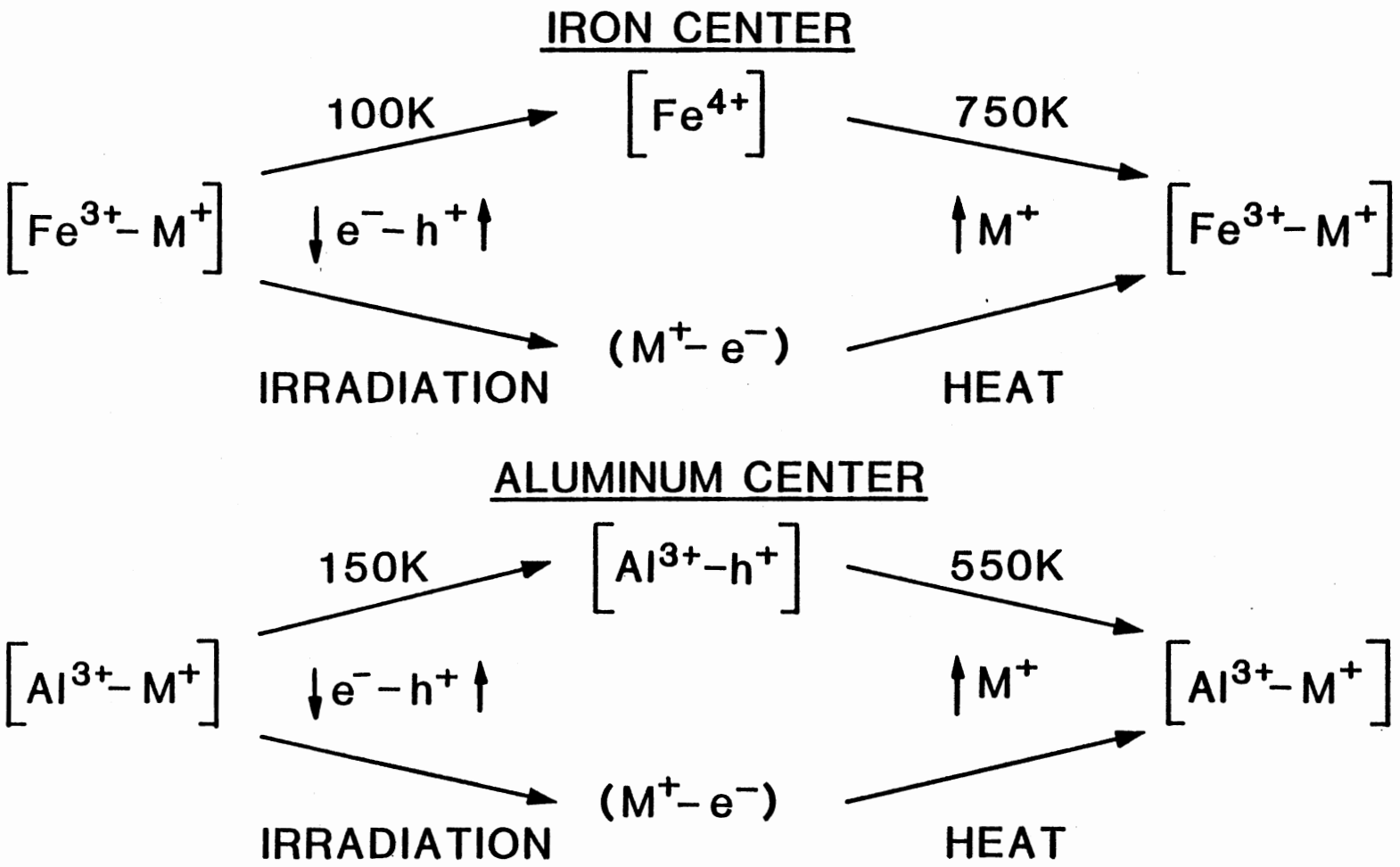

Figure 20. Schematic Representation of Iron and Aluminum Centers. Radiation-Induced Mobility of Alkali Interstitials

with the iron. Also, annealing experiments in different atmospheres could possibly be done.

A SELECTED BIBLIOGRAPHY

1. Eitel, W. The Physical Chemistry of the Silicates (University of Chicago Press, Chicago, 1954).

2. Laudise, R. A. and J. W. Nielsen. "Hydroghermal Crystal Growth", in Solid State Physics, edited by F. Seitz and D. Turnbull (Academic Press, New York, 1961), pp. 149-222.

3. Le Page, Y., L. D. Calvert, and E. J. Gabe, J. Phys. Chem. Solids 41, 721 (1980).

4. Halliburton, L. E., N. Koumvakalis, M. E. Markes, and J. J. Martin, J. Appl. Phys. 52, 3565 (1981).

5. Frondel, C. Dana's System of Mineralogy, Vol. 3 (Wiley and Sons, New York, 1962).

6. Halliburton, L. E., J. J. Martin, and D. R. Koehler. "Properties of Piezoelectric Materials", in Precision Frequency Control, edited by A. Ballato and E. Gerber (Academic Press, New York, in press), Chapter 1.

7. Fowler, W. B. Physics of Color Centers (Academic Press, New York, 1968).

8. Henderson, B. and J. E. Wertz. Defects in Alkaline-Earth Oxides (Taylor and Francis, Ltd., London, 1977).

9. Wertz, J. E. and J. R. Bolton. Electron Spin Resonance: Elementary Theory and Practical Applications (McGraw-Hill, New York, 1972).

10. Sibley, W. A., J. J. Martin, M. C. Wintersgill, and J. D. Brown, J. Appl. Phys. 50, 5449 (1979).

11. Doherty, S. P., J. J. Martin, A. F. Armington, and R. N. Brown, J. Appl. Phys. 51, 4164 (1980).

12. Markes, M. E. and L. E. Halliburton, J. Appl. Phys. 50, 8172 (1979).

13. Isoya, J., J. A. Weil, and P. H. Davis, J. Phys. Chem. Solids 44, 335 (1983).

14. Jani, M. G., R. B. Bossoli, and L. E. Halliburton, Phys. Rev. B 27, 2285 (1983).

15. Weeks, R. A., Phys. Rev. 130, 570 (1963).

16. Isoya, J., J. A. Weil, and L. E. Halliburton, J. Chem. Phys. 74, 5436 (1981).

17. Quoted in Reference 5, p. 180.

18. Brewster, R. F., Trans. Roy. Soc. Edinburg 9, i39 (1823).

19. Frondel, C., Am. Min. 19, 318 (1934).

20. Holden, H. A., Am. Min. 10, 203 (1925).

21. Cohen, A. J., Am. Min. 41, 874 (1956).

22. Bertheloff, R. V., C. R. 143, 477 (1906).

23. Hutton, D. R., Phys. Lett. 12, 310 (1964).

24. Hutton, D. R. and G. J. Troup, Nature 211, 621 (1966).

25. Barry, T. I. and W. J. Moore, Science 144, 289 (1964).

26. Barry, T. I., P. McNamara, and W. J. Moore, J. Chem. Phys. 42, 2559 (1965).

27. Matarrese, L. M., J. S. Wells, and R. L. Peterson, J. Chem. Phys. 50, 2350 (1969).

28. Lehmann, G. and W. J. Moore, J. Chem. Phys. 44, 1741 (1966).

29. Cox, R. T., J. Phys. C: Solid State Phys. 10, 4631 (1977).

VITA

Patrick E. Fisanich

Candidate for the Degree of

Master of Science

Thesis: EPR SPECTRA OF IRON CENTERS IN SYNTHETIC QUARTZ: RADIATION AND HEAT EFFECTS

Major Field: Physics

Biographical:

Personal Data: Born in Cheverly, Maryland, March 19, 1953.

Education: Graduated from Prince George's Community College, Largo, Maryland, with an Associates in Arts in Electronic Technology in 1974; received a Bachelor of Science in Physics in 1979 and a Master of Science in Mathematics in 1980, both from Lamar University, Beaumont, Texas. Completed the Master of Science at Oklahoma State University, Stillwater, Oklahoma, in December, 1983.